AIP | Journal of Applied Physics

Direct observation and mechanism of increased emission sites in Fe-coated microcrystalline diamond films

Kalpataru Panda, B. Sundaravel, B. K. Panigrahi, Pin-Chang Huang, Wen-Ching Shih, Huang-Chin Chen, and I-Nan Lin

Citation: Journal of Applied Physics **111**, 124309 (2012); doi: 10.1063/1.4729836
View online: http://dx.doi.org/10.1063/1.4729836
View Table of Contents: http://scitation.aip.org/content/aip/journal/jap/111/12?ver=pdfcov
Published by the AIP Publishing

Direct observation and mechanism of increased emission sites in Fe-coated microcrystalline diamond films

Kalpataru Panda,[1,a)] B. Sundaravel,[1] B. K. Panigrahi,[1,b)] Pin-Chang Huang,[2] Wen-Ching Shih,[2] Huang-Chin Chen,[3] and I-Nan Lin[3]
[1]*Materials Physics Division, Indira Gandhi Centre for Atomic Research, Kalpakkam 603 102, India*
[2]*Graduate Institute in Electro-Optical Engineering, Tatung University, Taipei 104, Taiwan*
[3]*Department of Physics, Tamkang University, New-Taipei 251, Taiwan*

(Received 27 February 2012; accepted 19 May 2012; published online 20 June 2012)

The electron field emission (EFE) properties of microcrystalline diamond (MCD) films are significantly enhanced due to the Fe coating and post-annealing processes. The 900 °C post-annealed Fe coated diamond films exhibit the best EFE properties, with a turn on field (E_0) of 3.42 V/μm and attain EFE current density (J_e) of 170 μA/cm^2 at 7.5 V/μm. Scanning tunnelling spectroscopy (STS) in current imaging tunnelling spectroscopy mode clearly shows the increased number density of emission sites in Fe-coated and post-annealed MCD films than the as-prepared ones. Emission is seen from the boundaries of the Fe (or Fe_3C) nanoparticles formed during the annealing process. In STS measurement, the normalized conductance $\frac{dI/dV}{I/V}$ versus V curves indicate nearly metallic band gap, at the boundaries of Fe (or Fe_3C) nanoparticles. Microstructural analysis indicates that the mechanism for improved EFE properties is due to the formation of nanographite that surrounds the Fe (or Fe_3C) nanoparticles. © *2012 American Institute of Physics*. [http://dx.doi.org/10.1063/1.4729836]

I. INTRODUCTION

Diamond films possess many desirable physical and chemical properties[1–3] and have been the focus of intensive research since the successful synthesis of diamond in the low pressure and low temperature chemical vapour deposition (CVD) process.[4] Diamond films have been extensively investigated for their application as electron field emitters due to their negative electron affinity (NEA) properties.[5] Generally, a good electron field emitter requires sufficient supply of electrons from the back contact materials, effective transport of electrons and efficient emission from the emitting sites. The large electronic band gap (5.5 eV) of diamond films hinder tremendously the electron field emission (EFE) behaviour due to lack of free electrons required for field emission process. Doping the diamond films with boron or nitrogen ions introduces new inter-band states within the band gap, which facilitates the easy transport of electrons from valence band to conduction band and thereby improving the EFE properties of these materials.[6] However, the EFE properties of these materials are still not satisfactory implying the fact that most of the sample surfaces do not have negative electron affinity characteristics because they are not re-constructed (100) surfaces. There are many efforts on modifying the surface of diamond films to increase the NEA characteristics. Among the approaches, a thin layer of metallic Fe coating on diamond films, followed by post-annealing in H_2 atmosphere significantly improves the EFE properties.[7–9] However, the related mechanism for improved EFE properties from these modified surfaces is still not clear.

In this context, we explore the possible reasons for the enhancement of EFE properties of these modified microcrystalline diamond (MCD) film surfaces, using scanning tunnelling spectroscopy (STS) in current imaging tunnelling spectroscopy (CITS) mode which determines the local electronic density of states (DOS) of the sample surfaces. We observed increased number density of emission sites for Fe coated and post-annealed MCD film surfaces than the as-prepared ones. High resolution transmission electron microscopy (HRTEM) was used to investigate the microstructural evolution of these films due to the Fe coating and subsequent annealing processes. Further, the possible mechanism for the enhancement in EFE is discussed on the basis of above experimental observations.

II. EXPERIMENTAL

Diamond films were grown on p-type silicon substrates with (100) orientation in microwave plasma enhanced chemical vapour deposition (IPLAS-Cyrannus) system. The substrates were first thoroughly cleaned by the standard RCA cleaning procedure,[10] which rinsed the Si wafer sequentially in water-diluted hydrogen peroxide/ammonium hydroxide and hydrogen peroxide/hydrochloric acid solution. Then, the substrates were preseeded by ultrasonication in a solution containing nanodiamond and titanium powder for 45 min to facilitate the nucleation of diamond. The substrates were again ultrasonicated in methanol solution to remove the possible adhered diamond and Ti nano-particles. The diamond films were grown in $CH_4/H_2 = 1/99$ sccm plasma excited by a 1400 W (2.45 GHz) microwave power with 55 Torr total pressure for 1 h. The MCD films were coated with a thin layer of iron (Fe) by DC sputtering process for 1 min to a thickness of around 10 nm. The Fe coated MCD films were then thermally post-annealed in H_2 atmosphere, with a flow rate of 100 sccm for 5 min with heating and cooling rates of around 15 °C/min. EFE properties of iron coated and post-annealed MCD films

[a)]Electronic mail: phy.kalpa@gmail.com.
[b)]Electronic mail: bkp@igcar.gov.in.

at lower temperatures (<800 °C) had already been studied by Huang *et al*., where not much improvement in EFE properties were observed.[9] Therefore, in the present study, we have selected three Fe coated and annealed MCD films at higher temperatures of 900°, 925°, and 950 °C to study the enhancement in EFE properties systematically. For simplicity, the Fe coated and annealed films were designated as $(Fe/MCD)_{900}$, $(Fe/MCD)_{925}$, and $(Fe/MCD)_{950}$, respectively.

Field emission measurements were carried out in a home built tuneable parallel plate capacitor setup. The separation of the anode (Mo) tip from the sample was measured using a digital micrometer and an optical microscope. The EFE properties were analyzed by the Fowler–Nordheim (F-N) model.[11]

$$J(E) = AE^2 \exp\left[\frac{-B\varphi^{3/2}}{E}\right], \text{with } A = e^3/16\pi^2 h\varphi t^2(y_0) \text{ and } B = 4/3e(2m/h^2)^{1/2}v(y_0)$$

where φ is the work function of the emitting material. J_e (in $\mu A/cm^2$) and E (in $V/\mu m$) are the EFE current density and applied field, respectively. The turn-on field was designated as the interception of the lines extrapolated from the high-field and low-field segments of F-N plots. The morphology and structure of the films were investigated by field emission scanning electron microscope (FESEM, CARL ZEISS, SUPRA 55). High resolution diffractometer (GIXRD—STOE) in 2θ range of 20°–90° at an angle of incidence 0.2° was used to detect the new phase formed due to the Fe coating and annealing process. The Raman spectra were recorded in back scattering geometry using 514.5 nm line of an Ar-ion laser using Renishaw micro-Raman spectrometer (Model-INVIA). The chemical bonding structures were investigated by x-ray photoelectron spectroscopy (XPS) using SPECS GmbH make photoelectron spectrometer which uses monochromatic Al Kα radiation at 1486.74 eV as a probe. This spectrometer with a monochromatic x-ray source has an energy resolution of 0.6 eV. The detailed microstructure of post-annealed Fe/MCD films was examined using high resolution transmission electron microscopy (HRTEM, Joel 2100).

Scanning tunnelling microscopy (STM) measurements were done in a commercial UHV-STM (150 Aarhus, SPECS GmbH) at a base pressure of 10^{-10} mbar. The tunnelling tips were prepared by electrochemical etching of tungsten tips of diameter 0.3 mm. The STS spectra were obtained during scanning and the data presented here are the average of many reproducible spectra acquired during subsequent scans. STS was also used in the CITS mode, which allows us to correlate the STM image with its surface local DOS distribution. CITS involves acquiring, a current versus voltage (I-V) curve, measured with the feedback loop off, in every point of the surface.[6]

III. RESULTS

A. General characteristics

Figure 1 shows the EFE properties of as-prepared and annealed Fe/MCD films. Inset in this figure shows the corresponding F-N plots. As seen from the current density versus electric field (J-E) curves, the EFE properties are significantly enhanced due to the Fe coating and annealing processes (Figures 1(ii) to 1(iv)), as compared with as-prepared MCD films (Fig. 1(i)). Better EFE properties are observed for $(Fe/MCD)_{900}$ (Fig. 1(iv)) films compared to $(Fe/MCD)_{925}$ (Fig. 1(iii)) and $(Fe/MCD)_{950}$ (Fig. 1(ii)) films. The turn-on field (E_0) decreased from 5.12 $V/\mu m$ (in case of as prepared MCD films) to 3.42 $V/\mu m$ for $(Fe/MCD)_{900}$ films. The E_0-values are 4.1 and 4.52 $V/\mu m$ for $(Fe/MCD)_{925}$ and $(Fe/MCD)_{950}$ films, respectively. Better current density (J_e) of 170 $\mu A/cm^2$ is measured for $(Fe/MCD)_{900}$ films at an electric field of 7.5 $V/\mu m$, while these values are 30 and 3 $\mu A/cm^2$ when annealing temperature increased to 925° and 950 °C, respectively, at the same electric field. The J_e value for as prepared MCD films is only 1.15 $\mu A/cm^2$ at 7.5 $V/\mu m$. The EFE properties of the samples are summarized in Table I.

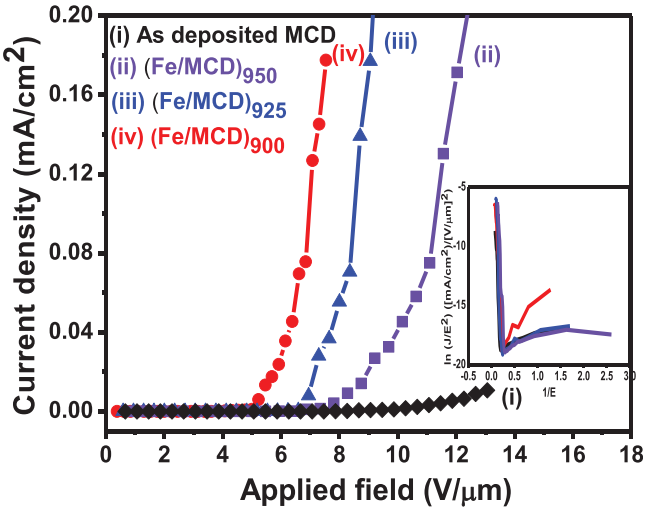

FIG. 1. The EFE properties for the (i) as-deposited MCD films. Fe-coated and post-annealed MCD films at (ii) 950 °C, (iii) 925 °C, (iv) 900 °C. Inset shows the F-N plot for the corresponding J-E curves.

The enhancement in EFE properties of Fe coated and post-annealed diamond films is due to the modification of the surface structures. The FESEM image of the Fe-coated/post annealed (900 °C) film, which shows best emission, is shown in Fig. 2. The inset in the figure shows the image of an as-prepared MCD film. Post-annealing processes tremendously alters the surface morphology of the Fe/MCD films. While the as-prepared MCD films contain large diamond grains about hundreds of nanometers with faceted geometry (inset of Fig. 2), annealing the Fe/MCD films at 900 °C forms nanoparticles of size 5–10 nm on the MCD surface as shown in

TABLE I. The EFE performances of as-prepared and Fe/MCD films annealed at different temperatures.

Samples	Turn-on field (E_0 in $V/\mu m$)	Current density at 7.5 $V/\mu m$ (J_e in $\mu A/cm^2$)
As prepared MCD film	5.12	1.15
$(Fe/MCD)_{900}$	3.42	170
$(Fe/MCD)_{925}$	4.10	30
$(Fe/MCD)_{950}$	4.52	3

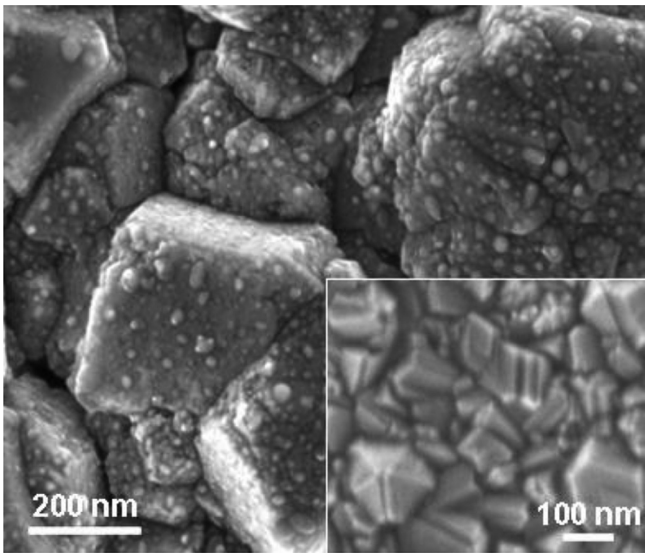

FIG. 2. SEM picture for Fe-coated and post-annealed (900 °C) MCD film with the inset showing the SEM picture of as-prepared MCD film.

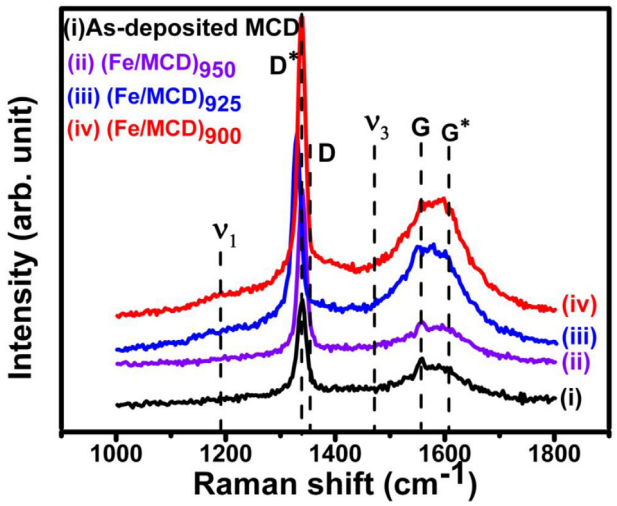

FIG. 4. Raman spectra of (i) as-deposited MCD film. MCD films after Fe-coating and annealing in (H_2) atmosphere at (ii) 950 °C, (iii) 925 °C, (iv) 900 °C.

Fig. 2. The GIXRD pattern of Fe/MCD films annealed at 900 °C (Fig. 3) shows three strongest peaks at 43.99°, 55.99°, and 75.48°, which correspond to the diamond (111), Fe_3C (212), and Fe_3C (322) phases, respectively.[12,13] The 5–10 nm particles seen on annealed Fe/MCD surfaces (SEM micrograph shown in Fig. 2) could be the Fe_3C nanoparticles. The faceted granular structure becomes slowly degraded when post-annealing temperature is increased to 925° and 950 °C (SEM micrographs not shown), respectively.

In order to understand how the annealing process modifies the chemical bonding state of the Fe coated MCD films, Raman and XPS measurements were carried out. Figure 4 shows the Raman spectra of as-grown and annealed Fe/MCD films. The Raman spectra are fitted with Lorentzian peaks with peak positions at 1191, 1339, 1357, 1470, 1559, and 1608 cm^{-1} which are marked as ν_1, D*, D, ν_3, G, and G*, respectively, in Fig. 4. D* is sharp and the dominant peak in all the films and it corresponds to F_{2g} zone center optical phonon of diamond indicating that MCD films are basically sp^3 bonded. The shift in wave number from 1332 to 1339 cm^{-1} is due to the stress in the films. ν_1 and ν_3 correspond to vibrations from trans-polyacetelene groups present at the grain boundaries. G peak is the characteristic of graphite (sp^2 bonded carbon) and G* corresponds to nanographite phase in the film surface. Since the Raman signal is several times sensitive to the sp^2-bonded carbon in comparison to the sp^3-bonded carbons, the presence of sp^2-related Raman resonance peaks does not imply the existence of a large proportion of sp^2-bonded materials in these MCD films. D peak corresponds to disordered carbon. It is due to the presence of amorphous carbon at the grain boundaries in as-deposited MCD films. The D-peak intensity is higher in case of Fe coated and post-annealed MCD films, indicating that there is some amorphous carbon at the Fe/diamond interface. A higher intensity of D-peak was observed in Fe/MCD samples annealed at lower temperatures (below 900 °C), whose field emission properties are poor compared with 900 °C annealed Fe/MCD samples.[9] This implies that amorphous carbon corresponding to D-peak is not a major contributor to the enhancement in the field emission properties. Also the intensities of G and G* peaks are higher in 900 °C annealed Fe/MCD samples. It is likely that nanographitic phase corresponding to G* peak plays significant role in the enhancement of field emission behaviour.[6] The Raman spectra of 950 °C annealed sample is similar to as-prepared MCD film, indicating that there is only a little amount of Fe left on the surface (which is confirmed with Rutherford backscattering spectrometry (not shown here)). The formation of Fe_3C and nanographitic phase on the film surface at high temperature annealed films (here at 900 °C) have significant role on the enhanced EFE properties, which will be discussed by TEM and XPS studies shortly. These results imply that the surface layer of diamond films is transformed to more sp^2-bonded graphite or amorphous carbon by Fe-coating, while the diamond material underneath has remained as such.

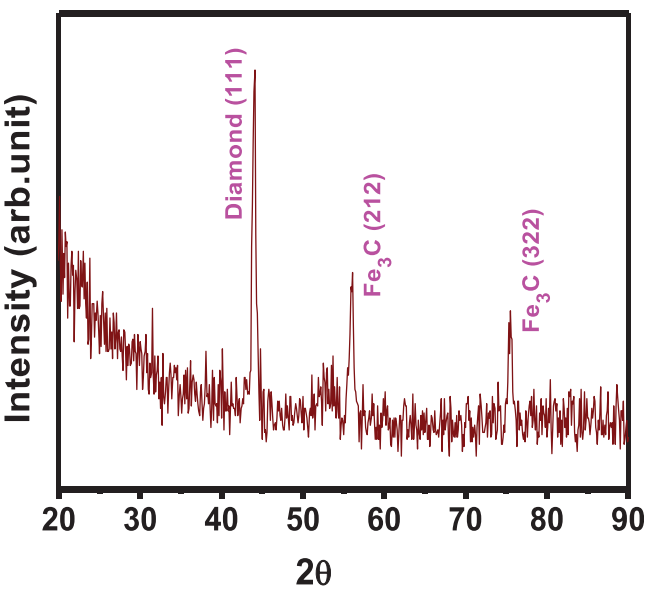

FIG. 3. GIXRD pattern of Fe coated MCD film post-annealed at 900 °C.

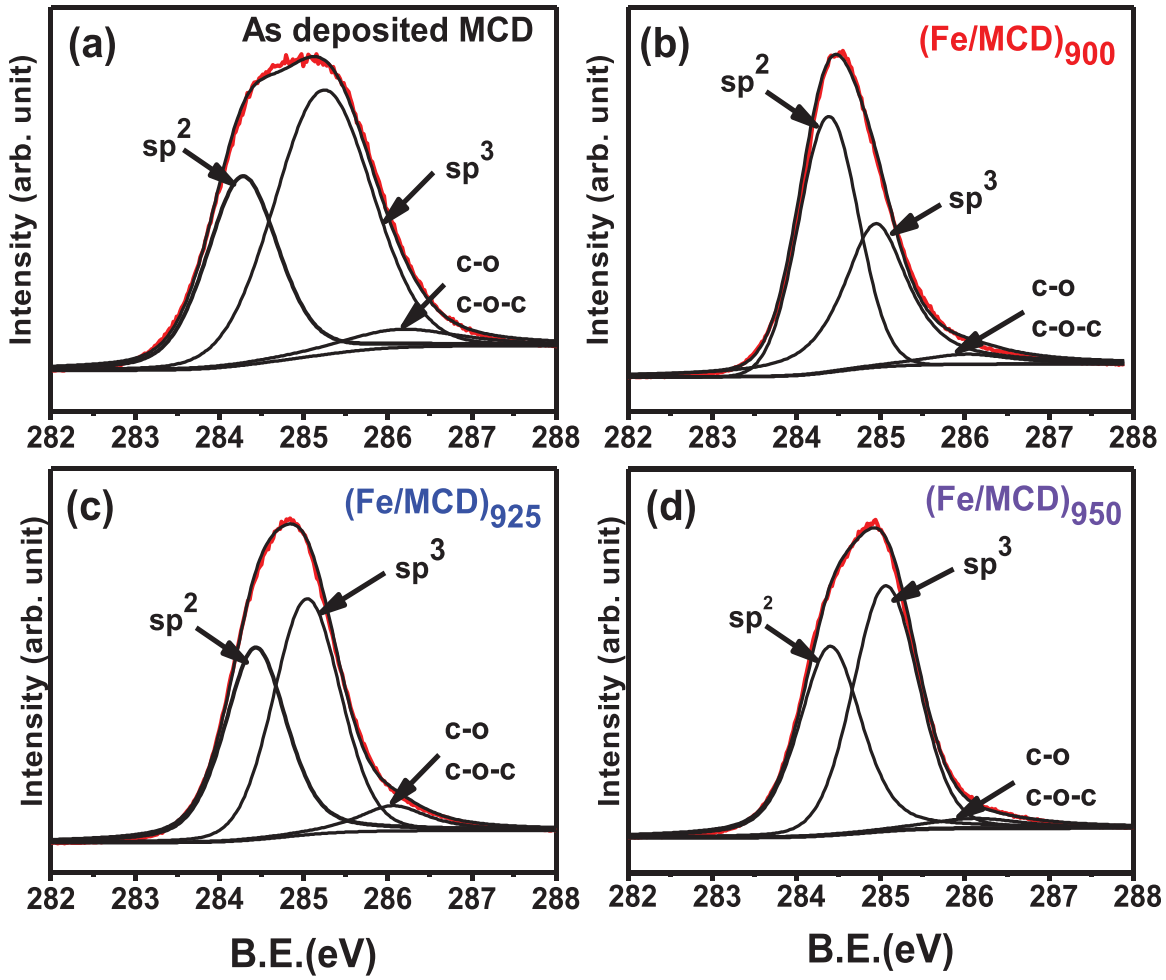

FIG. 5. XPS C1s spectra of (a) as-deposited MCD films. (b), (c), and (d) are Fe coated MCD films, which are annealed at different temperatures of 900 °C, 925 °C, and 950 °C, respectively.

The XPS C1s photoemission spectra of as-prepared MCD, $(Fe/MCD)_{900}$, $(Fe/MCD)_{925}$, and $(Fe/MCD)_{950}$ films are presented in Figs. 5(a)–5(d), respectively. The background was subtracted using Shirley's method.[14] XPS measurements were carried out without Ar-ion sputter etching to avoid reconfiguration of the surface bonding structures. The data were fitted with Lorentzian peaks with binding energies at 284.4, 285.0, and 286.1 eV corresponding to sp^2, sp^3 and C-O(C-O-C) bonding of the C1s spectra,[6] respectively. The relative intensities of each peak obtained from the C1s spectra are summarized in Table II. In C1s spectra of as-prepared MCD films, the sp^2 bonding is only 34.1%, while its concentration significantly increased to 52.4% after the Fe coating and annealing process in $(Fe/MCD)_{900}$ films. Further increase in annealing temperature degrades the sp^2 nature of these films. In contrast, the sp^3 phase was 60% in as-prepared films, compared with only 43.3% in $(Fe/MCD)_{900}$ films. Small CO/C–O–C peaks are seen in as prepared and annealed Fe/MCD films at binding energy of 286.1 eV, which disappears if surface is Ar-ion sputtered for one minute in the XPS chamber.

Figure 6 shows Fe2p XPS spectra of post-annealed Fe/MCD films. Strip marked areas represent the Fe $2p_{3/2}$ and $2p_{1/2}$ spectra. The data were fitted with Lorentzian peaks with binding energies at 707.0, 708.1, and 710.9 eV, corresponding to the Fe^0, Fe_3C, and Fe_2O_3 phases, respectively, of the Fe $2p_{3/2}$ peak.[15,16] The relative intensities of each peak obtained from the Fe $2p_{3/2}$ spectra are summarized in Table II. As shown in Fig. 6(a) and Table II, the peak intensities of Fe^0 and Fe_3C phases are 33.4% and 36.2% for $(Fe/MCD)_{900}$ films, 31.1% and 32.2% for $(Fe/MCD)_{925}$ (Fig. 6(b)) and 27.6%, 18.6% for $(Fe/MCD)_{950}$ (Fig. 6(c)) films, respectively. The concentrations of Fe and Fe_3C phases are more in $(Fe/MCD)_{900}$ films compared with higher

TABLE II. Relative intensities of various components of C 1s and Fe $2p_{3/2}$ in XPS spectra of as-prepared MCD, $(Fe/MCD)_{900}$, $(Fe/MCD)_{925}$ and $(Fe/MCD)_{950}$ films.

		Peak intensity (%)			
Peak position (eV)	Chemical bonding	As-prepared MCD	$(Fe/MCD)_{900}$	$(Fe/MCD)_{925}$	$(Fe/MCD)_{950}$
		C1s XPS			
284.4	sp^2	34.1	52.4	42.5	40.7
285.0	sp^3	60	43.3	50.2	54.1
286.1	C-O(or C-O-C)	5.9	4.3	7.3	5.2
707.0	Fe^0	…	33.4	31.1	27.6
708.1	Fe_3C	…	36.2	32.2	18.6
710.9	Fe_2O_3	…	30.4	36.7	53.8

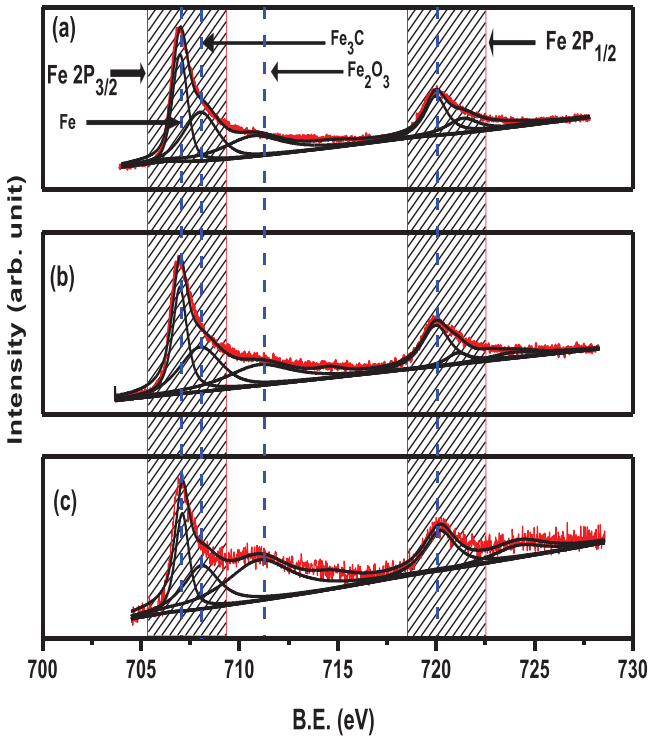

FIG. 6. XPS spectra for Fe 2p spectra of Fe coated MCD films, which are post annealed at different temperatures of (a) 900 °C, (b) 925 °C, (c) 950 °C.

temperature annealed, $(Fe/MCD)_{925}$ and $(Fe/MCD)_{950}$ films. Further increase in annealing temperature decreases the amount of Fe (or Fe_3C) phases and increases the Fe_2O_3 phase on the surface of diamond films, which degrades the EFE properties.[9] One possible reason for the presence of Fe_2O_3 phase is the oxidation of Fe-particles, which occurred instantaneously when the Fe coated MCD films were taken from the sputtering chamber to the annealing furnace. The increase in concentration of sp^2 and Fe (Fe_3C) phases are the factors responsible for the enhancement in EFE properties for these $(Fe/MCD)_{900}$ films.[6]

To understand the nature of nano-sized particles present on the surface of $(Fe/MCD)_{900}$ film, the detailed microstructure of the film was examined by TEM. It should be noted that, in the preparation of thin foil for TEM examination, the $(Fe/MCD)_{900}$ samples were ion-milled from the Si-side such that thin foil contains mainly the layer near the surface of the sample. Figure 7(a) shows a typical TEM micrograph of the $(Fe/MCD)_{900}$ film. Besides the large diamond grains, there are numerous ultra-small clusters (~5–10 nm) that are evenly distributed over the post-annealed Fe/MCD surface, which are also seen in SEM image shown in Fig. 2. Selected area electron diffraction (SAED) shown in inset of this figure indicates that the ultra-small clusters are randomly oriented Fe_3C clusters. There are rare, residual large Fe-particles distributed on the film surfaces. One of the Fe-particles is indicated by arrow in Fig. 7(a). Dark-field images were taken from a different part of SAED, i.e., from the diffraction spots corresponding to graphite, Fe, Fe_3C, and diamond separately, and the images were then superimposed to clearly illustrate the distribution of the phase constituents. Figure 7(b) shows the distribution of the nano-graphite (green color),

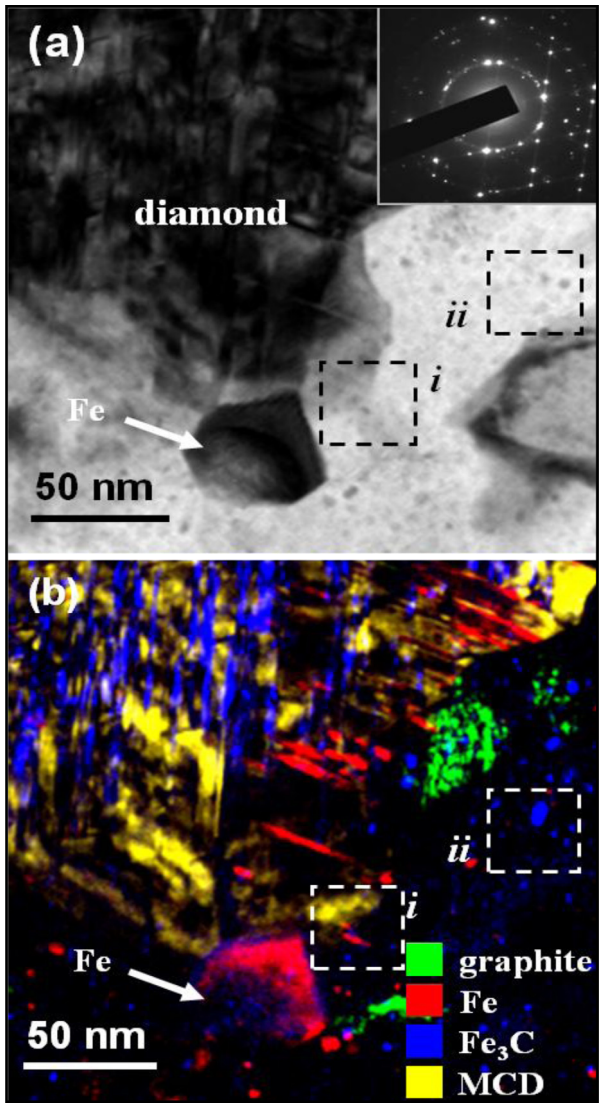

FIG. 7. The (a) bright field (BF) and (b) dark field (DF) TEM micrographs of a typical region in $(Fe/MCD)_{900}$ film.

Fe-particles (red color), and Fe_3C-clusters (blue color) contained in these films. The enlarged micrographs shown in Figures 8(a) and 8(b) reveal, respectively, the detailed microstructures of the region near the large diamond particle (area "*i*," Fig. 7(a)) and the small cluster region (area "*ii*," Fig. 7(a)) for the $(Fe/MCD)_{900}$ film. Figure 8(a) shows that the area 1 is diamond, as indicated by Fourier-transformed diffractogram (FT_1). In the region nearby the diamond grains, there exists an interaction zone about 5–10 nm in thickness. The FT image (FT_2) shown in Fig. 8(a) indicates that the interaction zone is of Fe_3C phase. Interestingly, there appears a graphitic phase about tens of nanometer in thickness outside the Fe_3C layer, which is indicated by the FT image FT_3. In contrast, Fig. 8(b) indicates that the small clusters contained in the region "*ii*" of Fig. 7(a) are mainly the smaller Fe_3C particles, which is highlighted by the area 4 and the FT image FT_4. There seems to be a thin layer of graphitic phase surrounding the small Fe_3C particles.

The presence of the nanographitic phase enhances the transport of electrons that facilitates the field emission

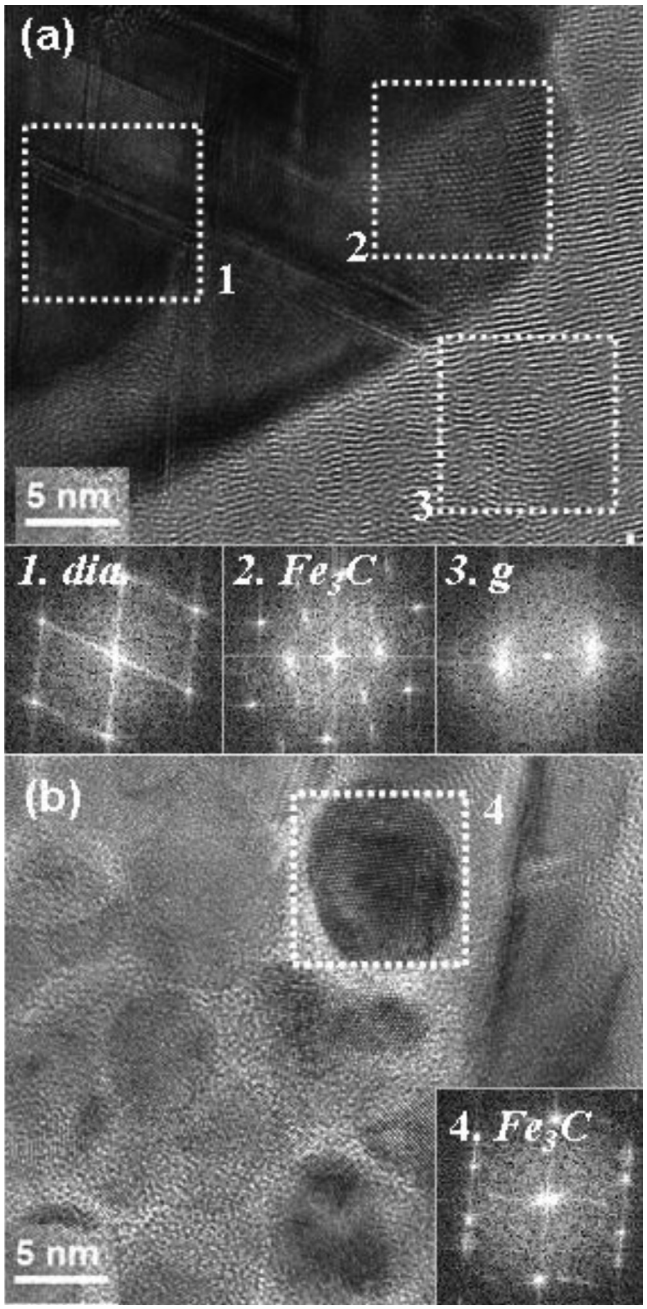

FIG. 8. The HRTEM micrographs corresponding to the (a) region "*i*" and (b) region "*ii*" in Fig. 7(a), showing the presence of Fe_3C particles and the associated graphitic layer. The insets show the Fourier-transformed diffractogram of the designated areas.

process, which is similar to the EFE properties of graphene composite.[17,18] The remaining unsolved question is how the nanographite is formed by the Fe-coating and post-annealing process. It has to be noted that the formation mechanism of carbon nanotubes (CNTs) has been proposed as follows: the carbon species is first dissolved into a catalyst and re-precipitated out, resulting in either a top-growth or bottom-growth process for CNTs.[19–22] The same dissolution and re-precipitation processes also occur for the nano-sized Fe-clusters formed on the diamond surface. Presumably, the Fe-clusters catalytically dissociated the diamond, transported the carbon species through the Fe-clusters, and reprecipitated them out at the other side of the clusters, resulting in nano-graphite on the surface of these Fe-clusters. The Fe_3C nano-clusters were resulted, when the Fe clusters containing some dissolved carbons are quickly cooled below the re-precipitation temperature.

B. Scanning tunnelling spectroscopy

For the purpose of understanding how the changes in concentrations of sp^2, sp^3, Fe (or Fe_3C) phases affect the EFE properties of these films, the local electronic properties of the films were investigated by STS. Only the STS measurements of the as-prepared and $(Fe/MCD)_{900}$ films are illustrated here. Figure 9(a) shows the image of as-prepared MCD film and its corresponding CITS image is shown in Fig. 9(b). Bright contrast in the CITS image shows better electron emission.[6] The CITS image of as prepared MCD film (Fig. 9(b)) shows that the emission is mostly from the facets of the micron-sized diamond grains. One such typical MCD grain and grain boundary are marked as "1" and "2," respectively, in Fig. 9(a) and the corresponding CITS image, taken at a bias of −3.5 V to the sample, is shown in Fig. 9(b), revealing the dark and bright contrast corresponding to the grain (point "1") and the grain boundary (point "2"), respectively. Thus, in as-prepared MCD films, only the facets of the diamond grains emit electrons.

In contrast, Fig. 9(c) shows the STM surface morphology of $(Fe/MCD)_{900}$ film and its corresponding CITS image, taken at the same bias of −3.5 V, is shown in Fig. 9(d). The CITS image in Fig. 9(d) clearly illustrates that, in comparison to the as-prepared MCD films, the emission sites are more in $(Fe/MCD)_{900}$ film surfaces. Typical diamond grain and grain boundary are marked as "3" and "4," respectively, in Fig. 9(c) and in its corresponding CITS image (Fig. 9(d)). The emission is seen from throughout the diamond grains in $(Fe/MCD)_{900}$ films rather than only from the facets of the diamond grains in the case of as-prepared MCD films.

To know more precisely how the Fe coating and post-annealing process enhances the number density of emission sites, the high resolution STM (HRSTM) and the corresponding CITS images are taken which are shown in Figs. 10(a) and 10(b), respectively. CITS image is taken at the same sample bias of −3.5 V. Again, bright contrast in CITS image indicates better electron emission. HRSTM picture shown in Fig. 10(a) reveals that the large diamond grains (shown in Fig. 9(c)) are actually composed of many nanometre sized particles of varying diameter from 5 to 20 nm. One typical bigger-sized particle (∼20 nm, marked as "5"), with its boundary marked as "6," is shown in Fig. 10(a). However, still smaller-sized particles of average size ∼5 nm could also be seen. Such a grain is marked as "7" and its boundary is marked as "8." Interestingly, the emission sites are seen from the boundaries of these bigger-sized (∼20 nm) and smaller-sized (∼5 nm) particles, as the corresponding CITS image (Fig. 10(b)) shows bright emission in the boundaries of these different sized nanoparticles (points "6" and "8"). Hence, we can conclude that in case of $(Fe/MCD)_{900}$ films, the micron-sized diamond grain consists of many nanoparticles of average grain size 5–20 nm. The boundaries of these nanoparticles emit and make interconnected path

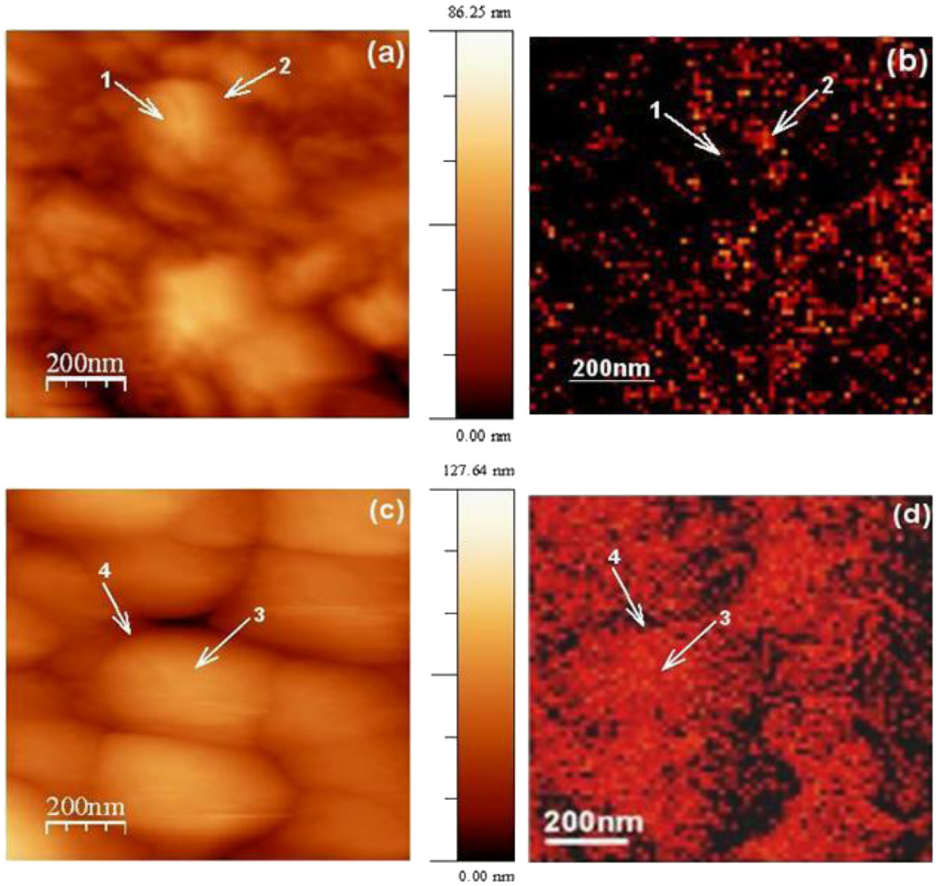

FIG. 9. (a) UHV STM image of as-deposited MCD films with the corresponding CITS image in (b). (c) Fe coated and post-annealed (900 °C) MCD film with corresponding CITS image in (d). The CITS images are taken in STS mode at a sample bias of −3.5 V. The increased emission sites after the Fe coating and annealing process is clearly seen in the CITS image (d) than (b).

throughout the film surfaces due to their high densities. The concentration of these nanoparticles is so much higher in $(Fe/MCD)_{900}$ films that it seems as if the whole micron-sized diamond grains emit in lower magnification scale (Fig. 9(d)).

For the characterization of the local electronic properties to get more insight into the nature of emission sites for the $(Fe/MCD)_{900}$ films, current-voltage (I–V) curves are taken in STS mode from various sample positions. The tunnelling current under positive bias is less than that under negative bias, implying that the films have n-type conductivity. Only the negative portion of the I–V curves is shown in Fig. 11(a) as the negatively biased current corresponds to the tunnelling of electrons from the diamond surface to the tungsten tip and is proportional to the density of occupied states of the diamond. Three reproducible I–V spectra were recorded during the scanning of the STM image. Conductivity at the boundaries surrounding the smaller-sized nano-particles (marked as "8" in Fig. 10(a)) and the bigger-sized nano-particles (marked as "6" in Fig. 10(a)) show ohmic behaviour (shown as curves "*i*" in Fig. 11(a)). Significant enhancement in conductivity has been observed (15 nA at −0.5 V) at these marked points. The smaller-sized nanoparticles (marked as "7" in Fig. 10(a)) also show high conductivity as shown in curves "*ii*" in Fig. 11(a), but it requires nearly about −1.0 V to attain the same 15 nA tunnelling current. These smaller particles could be the graphitic encapsulated Fe_3C particles, as shown in TEM observation. Some bigger-sized nano-particles marked as "5" in the HRSTM image Fig. 10(a) also show tunnelling current (curves "*iii*," Fig. 11(a)) but requires slightly more sample bias (−1.8 V) to attain the same

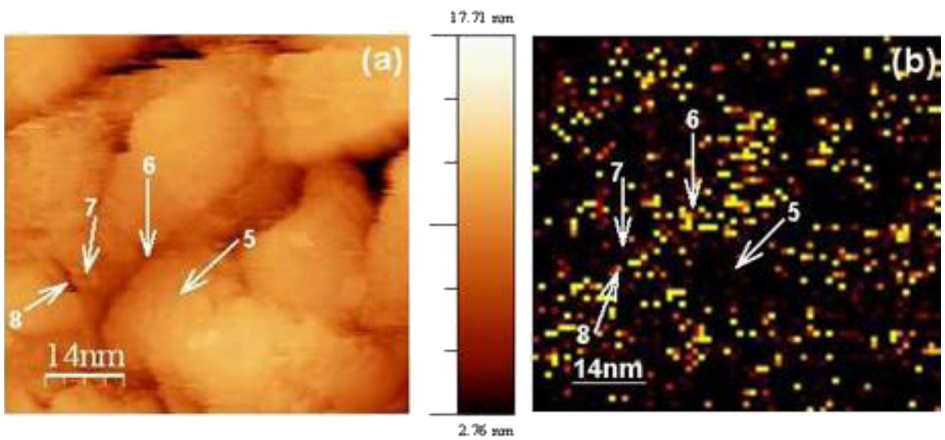

FIG. 10. (a) High resolution STM picture of Fe coated and post-annealed (900 °C) MCD film (b) corresponding CITS image taken in STS mode at a sample bias of −3.5 V.

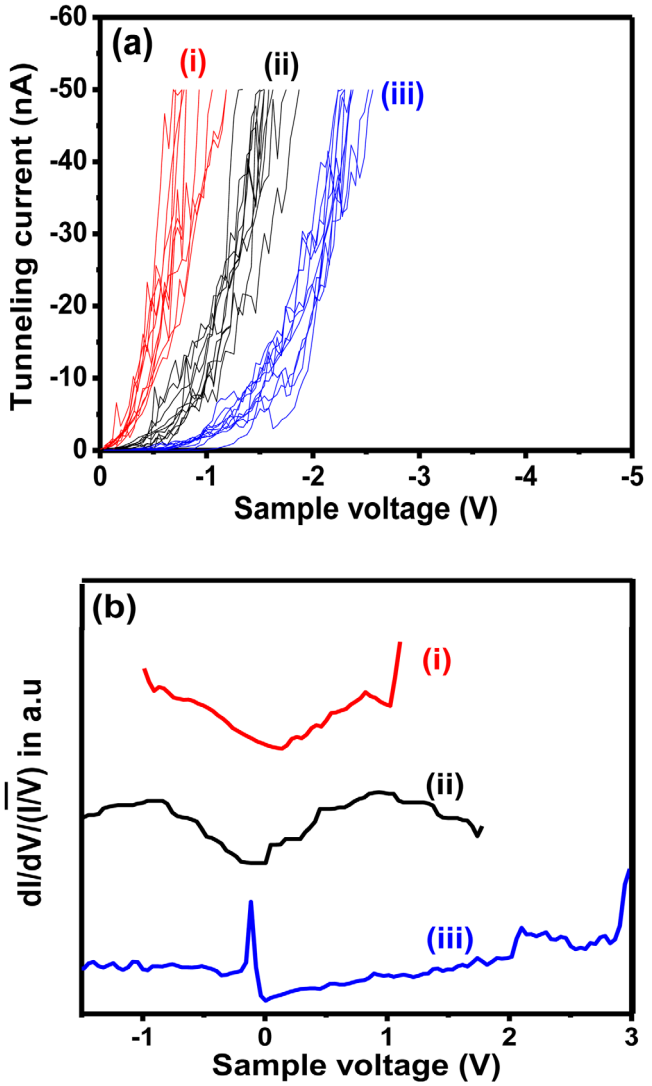

FIG. 11. (a) Tunnelling current vs. voltage (I–V) curves and (b) normalized differential conductance (dI/dV)/(I/V) curves at various locations: (i) at boundaries of nano-particles, marked as "6" and "8" in Fig. 10(a), (ii) on the smaller-sized (~5 nm) Fe_3C nanoparticles, marked as "7" in Fig. 10(a), and (iii) on the bigger-sized (20–25 nm) oxidized Fe nanoparticle, marked as "5" in Fig. 10(a).

(15 nA) tunnelling current. The local *I–V* characteristic curves at the facets of the as-prepared MCD grains (e.g., from area '2" in Fig. 9(a)) also show high conductivity as in the curves "*i*" shown in Fig. 11(a). It is to be noted here that for diamond grains in as prepared MCD films (e.g., '1" in Fig. 9(a)), it requires still higher bias voltage of −4.0 V to get the same value of (15 nA) tunnelling current. The behaviour of enhanced tunnelling current from the boundaries of Fe, Fe_3C nanoparticles in Fe coated and post-annealed films also explains the superior EFE properties in $(Fe/MCD)_{900}$ films than in the as prepared MCD in a microscopic scale.

The *I–V* characteristic curves of STS measurements shown in Fig. 11(a) are used to deduce the normalized derivative of multiple averaged spectra, the normalized conductance $\frac{dI/dV}{I/V}$. The normalized conductance spectra corresponding to the curves "*i*," "*ii*," and "*iii*" in Fig. 11(a) are plotted in Fig. 11(b), which provides information about the distribution of the surface density of states (DOS)[23,24] of the films. From the normalized conductance curve "*i*" in Fig. 11(b), nearly zero band gap (metallic type) is measured for the boundaries, which are marked as points "6" and "8" in the HRSTM image (cf. Fig. 8(a)). The nanographitic phase surrounding the Fe (bigger particles) or Fe_3C (smaller particles) nanoparticles (Figs. 8(a) and 8(b)) shows this metallic behavior. Band gap calculation on the smaller-sized (2–5 nm) particle also shows nearly metallic behavior (band gap 0.2 eV, curve "*ii*," Fig. 11(b)). It may be the graphitic layer encasing the smaller-sized Fe_3C nanoparticles. The smaller sized Fe_3C particles were formed by the reaction of Fe with diamond at high temperature of 900 °C, as evidenced by TEM observations. However, band gap calculation on the bigger-sized nanoparticle shows a gap value of 1.98 eV, as shown in the curve "*iii*" of Fig. 11(b). The large band gap in Fe particle may be due to the presence of thin oxide layer enveloping the Fe particle as a Fe_2O_3 phase, as evidenced from the XPS results shown in Fig. 6. Restated, the nanographitic phase present at the boundary of these Fe (or Fe_3C) nanoparticles seems to be the main conducting channel for electrons in addition to the facets. The formation of nanographitic phase can improve the EFE properties of diamond films, which have already been observed in the previous studies,[25,26] where the heavy-ion irradiation significantly enhances the EFE behaviour of materials via the induction of the nanographitic phase.

IV. DISCUSSION

Generally, in diamond films having micron-sized grains, electrons are transported along the grain boundaries and are emitted from these sites.[27,28] The density of emission sites is smaller for diamond films with larger grain size, as the emission comes from the facets of these micron sized diamond grains. STS in CITS mode shown in Fig. 9(b) reveals that the emission sites form a network of hundreds of nanometer in size. However, in $(Fe/MCD)_{900}$ films, the emission site density is large (cf. Fig. 9(d)). HRSTM image and its corresponding CITS image (cf. Figs. 10(a) and 10(b)) reveal that the boundaries of the Fe (or Fe_3C) nanoparticles make the interconnected paths for electron transport so that the emission site densities are significantly enhanced. The enhancement in EFE properties is thus accounted by the increased number density of emission sites in post-annealed $(Fe/MCD)_{900}$ films in a microscopic scale. Nanographitic phase is formed around the Fe (or Fe_3C) clusters and is presumed to serve as an electron transport medium as well as emission sites. Restated, in the Fe-coated/post-annealed MCD films, the emission sites form a network of approximately 5–10 nm in size (cf. Fig. 10(b)), which is markedly more abundant than the grain boundary network for as-prepared MCD films (cf. Fig. 9(b)). The increase in emission site densities explain the markedly larger EFE current density for the $(Fe/MCD)_{900}$ films $[(J_e)_{Fe/MCD} = 170\ \mu A/cm^2$ at 7.5 V/μm for $(Fe/MCD)_{900}$ films whereas $(J_e)_{MCD} = 1.15\ \mu A/cm^2$ for as-grown MCD films]. It seems that different sized nano particles encased with nanographitic phase, formed by the reaction of Fe with the diamond at 900 °C annealing temperature, play a significant role in EFE properties of these films.

It is also noted here that the reaction between Fe and diamond does not occur at temperature below 800 °C, no matter how long the reaction time is, but will be triggered instantaneously at higher temperature of above 850 °C, even for a very short post-annealing time of 5 min. Band gap calculations from STS data, at the boundaries of these smaller (2–5 nm) and bigger (20 nm) particles show metallic nature implying that these are the nanographitic phase surrounding these nanoparticles, which is also evidenced from the HRTEM study. The smaller (~5 nm) particles are the Fe_3C, whereas the bigger (~20 nm) particles are the Fe-clusters. Therefore, in $(Fe/MCD)_{900}$ films, EFE properties are significant because of the presence of high concentration of Fe, Fe_3C nanoparticles throughout the film's surface, whose boundaries are encased with nanographitic phase.

V. CONCLUSION

Fe-coating and post-annealing processes at high temperatures have been observed to markedly modify the surface characteristics and enhance the EFE properties of MCD films. The evolution of surface morphology and structure with post-annealing temperature was investigated in detail. XPS measurements show the sp^2 phase fraction and concentration of Fe (or Fe_3C) phases are more in 900 °C post-annealed Fe coated MCD films, which possesses the best EFE properties. STS in CITS mode clearly shows the increased number densities of emission sites in $(Fe/MCD)_{900}$ films than the as-deposited ones. I–V curves show ohmic behaviour, whereas $\frac{dI/dV}{I/V}$ versus V curves show nearly metallic band gap, at the grain boundaries of Fe (or Fe_3C) nanoparticles, as seen from STS measurements. Microstructural analysis indicates that the mechanism for the improvement of the EFE process is the formation of nanographitic phase at the boundaries of the Fe (or Fe_3C) nanoparticles, which are formed via the reaction of Fe clusters with diamond films during the annealing process. The nanographitic phase was formed by the re-precipitation of carbon species, which is dissolved in the Fe clusters, in a process similar to the growth of carbon nanotubes via Fe clusters as catalyst.

ACKNOWLEDGMENTS

The authors would like to thank Mr. Nandagopala Krishna for XPS, Mr. P. Shyamala Rao for FESEM, Sujoy Chakravarty of UGC-DAE CSIR, Kalpakkam for GIXRD and the National Science Council, Republic of China for the support of this research through the Project No. NSC 99-2119 -M-032- 003-MY2. Authors would like to thank Dr. C. S. Sundar, Director, Materials Science Group, Indira Gandhi Centre for Atomic Research for his sustained encouragement and consistent support.

[1]J. E. Field, *The Properties of Diamonds* (Academic, London, 1979).
[2]H. Liu and D. S. Dandy, Diamond Relat. Mater. **4**, 1173 (1995).
[3]J. C. Angus, H. A. Will, and W. S. Stanko, J. Appl. Phys. **39**, 2915 (1968).
[4]B. V. Spitsyn, L. L. Bouilov, and B. V. Derjaguin, J. Cryst. Growth **52**, 219 (1981).
[5]F. J. Himpsel, J. A. Knapp, J. A. Van Vechten, D. E. Eastman, Phys. Rev. B **20**, 624 (1979).
[6]K. Panda, B. Sundaravel, B. K. Panigrahi, P. Magudapathy, D. N. Krishna, K. G. M. Nair, H-C. Chen, and I-Nan Lin, J. Appl. Phys. **110**, 044304 (2011).
[7]A. Lamouri, Y. Wang, G. T. Mearini, I. L. Krainsky, J. A. Dayton, Jr., and W. Mueller, J. Vac. Sci. Technol. B **14**, 2046 (1996).
[8]I. N. Lin, Y. H. Chen, and H. F. Cheng, Diamond Relat. Mater. **9**, 1574 (2000).
[9]P. C. Huang, W. C. Shih, H. C. Chen, and I. N. Lin, JJAP Ser. **50**, 08KE04 (2011).
[10]W. Kern, J. Electrochem. Soc. **137**, 1887 (1990).
[11]R. H. Fowler and L. Nordheim, Proc. R. Soc. London, Ser. A **119**, 173 (1928).
[12]J. Thewlis and A. R. Davey, Phys. Rev. B, **49**, 9341 (1994).
[13]E. J. Fasika and G. A. Jeffrey, Acta Crystallogr. **19**, 463 (1965).
[14]Y. F. Chen, Surf. Sci. **380**, 199 (1997).
[15]Yang Kai-Yu, Xu Wei, Zhang Yu, Zheng Wei-Tao, and Wang Xin, Chem. Res. Chin. Univ. **26**(3), 348 (2010).
[16]T. Fujii, F. M. F. de Groot, and G. A. Sawatzky, Phys. Rev. B, **59**, 4 (1999).
[17]G. Eda, H. E. Unalan, N. Rupesinghe, G. A. J. Amaratunga, and M. Chhowalla, Appl. Phys. Lett. **93**, 233502 (2008).
[18]Z. S. Wu, S. Pei, W. Ren, D. Tang, L. Gao, B. Liu, F. Li, C. Liu, and H. M. Cheng, Adv. Mater. **21**, 1756 (2009).
[19]D. C. Li, L. Dai, S. Huang, A. W. H. Mau, and Z. L. Wang, Chem. Phys. Lett. **316**, 349 (2000).
[20]E. F. Kukovitsky, S. G. L'vov, and N. A. Sainov, Chem. Phys. Lett. **317**, 65 (2000).
[21]S. B. Sinnott, R. Andrews, D. Qian, A. M. Rao, Z. Mao, E. C. Dickey, and F. Derbyshire, Chem. Phys. Lett. **315**, 25 (1999).
[22]A. Gorbunov, O. Jost, W. Pompe, and A. Graff, Carbon **40**, 113 (2002).
[23]R. M. Feenstra, Surf. Sci. **965**, 299 (1994).
[24]R. M. Feenstra and P. Martenssion, Phys. Rev. Lett. **61**, 4 (1988).
[25]H. C. Chen, U. Palnitkar, W. F. Pong, I. N. Lin, A. P. Singh, and R. Kumar, J. Appl. Phys. **105**, 083707 (2009).
[26]H. C. Chen, K. Y. Teng, C. Y. Tang, B. Sundaravel, S. Amirthapandian, and I. N. Lin, J. Appl. Phys. **108**, 123712 (2010).
[27]M. W. Geis, N. N. Efremow, J. D. Woodhouse, M. D. Mcaleese, M. Marchywka, D. G. Socker, and J. F. Hochedez, IEEE Electron Device Lett. **12**, 456 (1991).
[28]R. Krauss, O. Auciello, M. Q. Ding, D. M. Gruen, Y. Huang, V. V. Zhirnov, E. I. Givargizov, A. Breskin, R. Chechen, E. Shefer, V. Konov, S. Pimenov, A. Karabutov, A. Rakhimov, and N. SuetinL, J. Appl. Phys. **89**, 2598 (2001).